

See discussions, stats, and author profiles for this publication at: <https://www.researchgate.net/publication/359204559>

On the mathematical and numerical treatment of polydisperse sedimentation

Conference Paper · March 2022

CITATIONS

0

READS

60

2 authors:



Raimund Bürger
Universidad de Concepción, Concepción, Chile
281 PUBLICATIONS 5,556 CITATIONS

[SEE PROFILE](#)



Victor Osores
Universidad Católica del Maule
9 PUBLICATIONS 28 CITATIONS

[SEE PROFILE](#)

On the mathematical and numerical treatment of polydisperse sedimentation

Raimund Bürger

Víctor Osores

Full Professor

Doctoral Student

CI²MA & Depto. de Ingeniería Matemática
Universidad de Concepción
Casilla 160-C, Concepción, Chile
rburger@ing-mat.udec.cl

CI²MA & Depto. de Ingeniería Matemática
Universidad de Concepción
Casilla 160-C, Concepción, Chile
victorosores@udec.cl

Key words : Polydisperse sedimentation, hyperbolicity, convection-diffusion system, IMEX schemes, multilayer shallow-water system

AMS Mathematics Subject Classification : 2010 AMS Subject Classification Number:
35K59, 35L65, 65L06, 65M06, 65M08, 76T20

Abstract : We review some recent advances in the mathematical modelling and numerical simulation of polydisperse suspensions of small particles dispersed in a viscous fluid. Such a mixture contains small particles of multiple species that differ in size or density, and that segregate and form areas of different composition. In one space dimension, common models that describe the settling as such mixtures, and that generalize the well-known kinematic theory of sedimentation [38], can be formulated as systems of first-order nonlinear conservation laws for the unknown volume fractions as functions of height and time. These models differ in the algebraic form of the flux vector. One of the models that has received major acceptance through extensive support by experimental data was proposed by Masliyah [41] and Lockett and Bassoon [40] (“MLB model”). Several properties of these models are discussed. Of particular theoretical and practical interest is the property of hyperbolicity, that is, the existence of pairwise distinct real eigenvalues and a full set of corresponding eigenvectors of the flux Jacobian. This property is related to the stability of the sedimentation process and allows the implementation of high-resolution numerical schemes for its simulation. The spectral decomposition required to identify conditions for hyperbolicity is not available in closed form but can be characterized by the approach of the so-called secular equation [3, 17]. The MLB and related models have been extended to describe suspensions forming compressible sediments. In that case, the governing equation is a system of nonlinear degenerate convection-diffusion type. The numerical solution of such models by explicit schemes is usually very inefficient due to the severe time step restriction. A more efficient, and still easy-to-implement alternative are so-called implicit-explicit numerical schemes (“IMEX schemes”) that treat the convective part by an explicit scheme, and the nonlinear diffusive part by an implicit scheme [13, 14]. Finally, an outlook on some current developments, and in particular on spatially multi-dimensional models will be given [22].

1 Introduction

1.1 Scope

We are interested in the process of sedimentation of small solid particles in a viscous fluid under the influence of gravity, as is illustrated in Figure 1 for a monodisperse suspension, that is, for which the solid particles have equal size and density. Standard references to simple kinematic models that describe the settling of such a mixture include [26, 28, 38]. We herein focus on so-called polydisperse suspensions, in

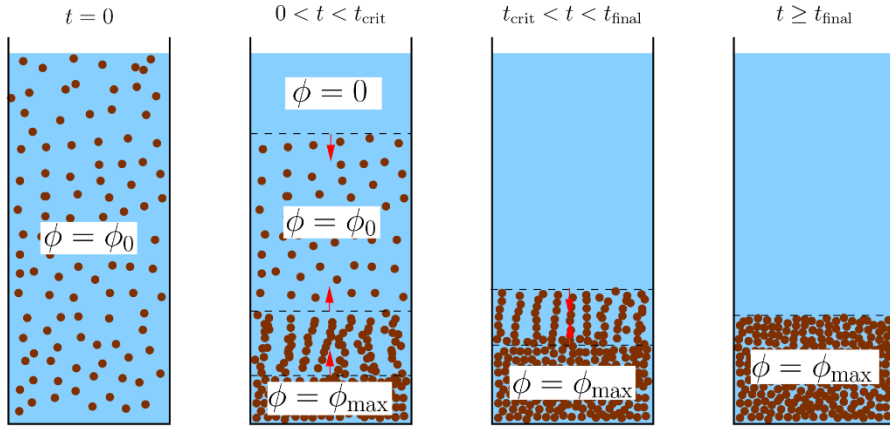


Fig. 1: Schematic of the sedimentation of a monodisperse suspension of small solid particles in a viscous fluid: (left) suspension at initial solids volume fraction ϕ_0 , (middle left) formation of a clear liquid (supernatant) region ($\phi = 0$) and a densely packed sediment ($\phi = \phi_{\max}$), showing a descending suspension-supernatant interface and a rising sediment-suspension interface, which meet at a critical time t_{crit} , (middle right) compaction of the sediment after critical time t_{crit} , but before the system has attained steady state, (right) final steady state with particles at rest and sediment at maximum packing solids volume fraction ϕ_{\max} .

which the solid particles belong to a finite number of classes (species) that have different sizes and densities. The different species segregate and form areas of different composition. In many applications, a spatially one-dimensional description of this process, with the space coordinate aligned with the body force (usually gravity) is sufficient. The mathematical frame of continuum descriptions of that kind is given by first-order systems of nonlinear conservation laws [11, 17, 21] whenever sediment compressibility is not in effect. Applications of spatially one-dimensional polydisperse sedimentation models are reviewed in [12]. They include geophysics [2, 30, 31, 50], chemical engineering [1, 43], mineral processing [36], medicine [45], petroleum engineering [33], wastewater treatment [16, 47, 51], and other areas. The systems of conservation laws arising in these applications are of arbitrary size (namely, of N scalar equations for N unknowns, that is, the N volume fractions ϕ_1, \dots, ϕ_N as a function of position x and time t if we distinguish N solid particle species), but their fluxes are constructed in a systematic way. In some important cases it is the possible to prove that the resulting system is strictly hyperbolic for equal-density particles [17, 19]. The flux Jacobian does not admit a closed-form eigenstructure, but spectral schemes can still be implemented [18].

For the convective flow of a particulate suspension (e.g., in rivers and estuaries), that is for the description of vertical sedimentation superposed with a horizontal flow, two- or three-dimensional models are needed. These are computationally expensive since additional equations of motion need to be solved. However, certain simplification is possible for suspended sediment transport in shallow regimes, which can be described by a Saint-Venant or shallow water model combined with passive transport equations for the different species. We herein consider a related model, namely a multilayer shallow water model for polydisperse sedimentation.

1.2 Model of polydisperse sedimentation

Let us first consider a multi-dimensional setup, where \mathbf{x} denotes spatial position. It is assumed that the polydisperse suspensions consists of spherical solid particles that belong to N species of sizes $d_1 \geq \dots \geq d_N$ and densities ρ_1, \dots, ρ_N with the corresponding volume fractions $\phi_i = \phi_i(\mathbf{x}, t)$, $i = 1, \dots, N$. Moreover, we define the total solids volume fraction $\phi := \phi_1 + \dots + \phi_N$, where it is usually assumed that $0 \leq \phi \leq \phi_{\max}$, where ϕ_{\max} is a maximum packing density. This description presupposes that the particle sizes are relatively small, at least with respect to the diameter of the settling vessel, so that a continuum description is adequate

but on the other hand colloidal effects are unimportant. Moreover, it is assumed that the fluid has density ρ_f and viscosity μ_f . If g denotes the acceleration of gravity, then the derived parameters used for the model formulation are

$$\mu = -\frac{gd_1^2}{18\mu_f}, \quad \delta_j = \frac{d_j^2}{d_1^2}, \quad \bar{\rho}_j = \rho_j - \rho_f, \quad \bar{\rho} = \begin{pmatrix} \bar{\rho}_1 \\ \vdots \\ \bar{\rho}_N \end{pmatrix}, \quad \delta = \begin{pmatrix} \delta_1 = 1 \\ \delta_2 \\ \vdots \\ \delta_N \end{pmatrix}, \quad \Phi = \begin{pmatrix} \phi_1 \\ \vdots \\ \phi_N \end{pmatrix}.$$

To formulate the balance equations in multiple dimensions, let us assume that $j = 0$ corresponds to the fluid and $j = 1, \dots, N$ to the solid phases. We then obtain

$$\partial_t \phi_j + \nabla \cdot (\phi_j \mathbf{v}_j) = 0, \quad j = 0, \dots, N, \quad (1.1)$$

$$\nabla \cdot \mathbf{q} = 0, \quad (1.2)$$

$$\rho_j (\partial_t (\phi_j \mathbf{v}_j) + \nabla \cdot (\phi_j \mathbf{v}_j \otimes \mathbf{v}_j)) = -\rho_j \phi_j g \mathbf{e}_z - \phi_j \nabla p, \quad j = 1, \dots, N, \quad (1.3)$$

where \mathbf{v}_j is the phase velocity of phase j ($j = 0, 1, \dots, N$), \mathbf{e}_z is the upward-pointing unit vector, and p is the pressure. The solids phase velocities are given by

$$\mathbf{v}_j = \mathbf{q} + v_j^{\text{MLB}}(\Phi) \mathbf{e}_z, \quad j = 1, \dots, N,$$

where v_j^{MLB} is the hindered settling function corresponding to the model introduced independently by Masliyah [41] and Lockett and Bassoon [40] (“MLB model”), namely

$$v_j^{\text{MLB}}(\Phi) = \mu V(\phi) \left[\delta_j (\bar{\rho}_j - \bar{\rho}^T \Phi) - \sum_{l=1}^N \delta_l \phi_l (\bar{\rho}_l - \bar{\rho}^T \Phi) \right], \quad (1.4)$$

where V is a given function, sometimes called “hindered settling factor”, that is assumed to satisfy

$$V(0) = 1, \quad V(\phi_{\max}) = 0, \quad V'(\phi) \leq 0.$$

Finally, we remark that if the phase velocity \mathbf{v}_j has a horizontal component \mathbf{u}_j and a vertical component ϖ_j , $j = 0, \dots, N$, then we assume that $\mathbf{u}_0 = \mathbf{u}_1 = \dots = \mathbf{u}_N =: \mathbf{u}$.

1.3 Special cases

If the particle species have equal density ρ_s (and differ in size only), then (1.4) reduces to

$$v_j^{\text{MLB}} = \mu V(\phi) (1 - \phi) (\rho_s - \rho_f) [\delta_j - \delta^T \Phi]. \quad (1.5)$$

Furthermore, in one space dimension, (1.2) implies that $\mathbf{q} = q$ is constant, with $q = 0$ for batch settling. Thus, for the description of settling in a column of height L we only need to solve the zero-flux initial-boundary value problem

$$\begin{aligned} \partial_t \Phi + \partial_x \mathbf{f}(\Phi) &= \mathbf{0}, \quad \mathbf{f}(\Phi) = (f_j(\Phi))_{j=1}^N, \quad f_j(\Phi) = \phi_j v_j(\Phi), \\ \Phi(x, 0) &= \Phi_0(x), \quad 0 \leq x \leq L; \quad \mathbf{f}(\Phi)|_{x=0} = \mathbf{f}(\Phi)|_{x=L} = \mathbf{0}. \end{aligned} \quad (\text{BSM})$$

This is a first-order nonlinear system of conservation laws whose solutions exhibit kinematic shocks (concentration discontinuities), in agreement with experimental evidence [46]. This model is discussed in Section 2.

On the other hand, if we still consider the one-dimensional case but assume that the sediment is compressible, then the governing model can be written as

$$\partial_t \Phi + \partial_x \mathbf{f}(\Phi) = \partial_x (\mathbf{B}(\Phi) \partial_x \Phi), \quad (\text{DCM})$$

$$\Phi(x, 0) = \Phi_0(x), \quad 0 \leq x \leq L; \quad \mathbf{f}(\Phi) - \mathbf{B}(\Phi) \partial_x \Phi|_{x=0,L} = \mathbf{0},$$

where the term $\partial_x(\mathbf{B}(\Phi)\partial_x\Phi)$ describes a diffusive correction (DC) of the original kinematic model (see [11, 13, 14]). The diffusion matrix $\mathbf{B}(\Phi) = (\beta_{ij}(\Phi))_{i,j=1,\dots,N}$ has the structure

$$\beta_{ij}(\Phi) = \gamma_{ij}(\Phi)\sigma_e(\phi) + \alpha_{ij}(\Phi)\sigma'_e(\phi)$$

with certain coefficient functions γ_{ij} and $\alpha_{ij}(\Phi)$ (whose precise algebraic definition is unimportant here), and where σ_e denotes the so-called effective solid stress function that has the generic property

$$\sigma_e(\phi), \sigma'_e(\phi) \begin{cases} = 0 & \text{for } \phi \leq \phi_c, \\ > 0 & \text{for } \phi > \phi_c, \end{cases} \quad \sigma'_e(\phi) \text{ jumps at } \phi_c, \quad (1.6)$$

corresponding to the assumption that effective solid stress can only be transmitted when the particles are in permanent contact, which in turn is assumed to occur when the total volume fraction ϕ exceeds a critical value ϕ_c , sometimes called “gel point”. Clearly, under the assumption (1.6), the partial differential equation (PDE) in (DCM) is strongly degenerate. In fact, one can show [11] that the PDE of (DCM) is parabolic wherever $\sigma_e(\phi)$ is active. This model is discussed in Section 3.

Finally, we consider an alternative formulation based on mass averaging. We define

$$\rho := \rho(\Phi) := \rho_0\phi_0 + \rho_1\phi_1 + \cdots + \rho_N\phi_N. \quad (1.7)$$

Then the mass average velocity of the mixture

$$\mathbf{v} := (u, v, w)^T := \frac{1}{\rho} \sum_{m=0}^N \rho_m \phi_m \mathbf{v}_m = \frac{1}{\rho} \left[\left(\rho - \sum_{j=1}^N \rho_j \phi_j \right) \mathbf{v}_0 + \sum_{k=1}^N \rho_k \phi_k \mathbf{v}_k \right]$$

satisfies the global mass balance $\partial_t \rho + \nabla \cdot (\rho \mathbf{v}) = 0$. If we define the slip velocities $\mathbf{u}_i := \mathbf{v}_i - \mathbf{v}_0$ and the factor $\lambda_i := \rho_i \phi_i / \rho$ for $i = 1, \dots, N$, then the solids mass balance equations can be rewritten as

$$\partial_t \phi_j + \nabla \cdot \left(\phi_j \left(\mathbf{u}_j + \mathbf{v} - \sum_{l=1}^N \lambda_l \mathbf{u}_l \right) \right) = 0, \quad j = 1, \dots, N. \quad (1.8)$$

The governing model in final form is

$$\partial_t(\rho_j \phi_j) + \nabla \cdot (\rho_j \phi_j \mathbf{v}_j) = 0, \quad j = 1, \dots, N, \quad (1.9)$$

$$\rho_j(\partial_t(\phi_j \mathbf{v}_j) + \nabla \cdot (\phi_j \mathbf{v}_j \otimes \mathbf{v}_j)) = \nabla \cdot \mathbf{T}_j^E - \phi_j \nabla p - \phi_j \rho g \mathbf{k}, \quad j = 1, \dots, N, \quad (1.10)$$

$$\partial_t \rho + \nabla \cdot (\rho \mathbf{v}) = 0, \quad (1.11)$$

where

$$\mathbf{v}_j = \mathbf{v} + \tilde{v}_j^{\text{MLB}}(\Phi) \mathbf{e}_z, \quad \tilde{v}_j^{\text{MLB}}(\Phi) := \mu V(\phi) \left[\delta_j(\bar{\rho}_j - \bar{\rho}^T \Phi) - \sum_{l=1}^N \lambda_l \delta_l \phi_l (\bar{\rho}_l - \bar{\rho}^T \Phi) \right]. \quad (1.12)$$

Summing up from 0 to N the equations (1.10) we have

$$\partial_t \left(\sum_{j=0}^N \rho_j \phi_j \mathbf{v}_j \right) + \nabla \cdot \left(\sum_{j=0}^N \rho_j \phi_j \mathbf{v}_j \otimes \mathbf{v}_j \right) = \nabla \cdot \mathbf{T} - \rho g \mathbf{k}, \quad (1.13)$$

where the stress tensor of the mixture is given by

$$\mathbf{T} = \sum_{j=0}^N T_j = -p \mathbf{I} + \mathbf{T}^E.$$

This model forms the basis of a multilayer shallow water formulation that is discussed in Section 4.

2 Hyperbolicity and characteristic schemes

It is possible to analyze the hyperbolicity for (BSM) and a wide class of models of the settling velocities v_i (including the MLB model) by the approach of the so-called secular equation [3], see [17, 19, 29], where we recall that the system of conservation laws

$$\partial_t \Phi + \partial_x \mathbf{f}(\Phi) = \mathbf{0} \quad (2.1)$$

is called *hyperbolic* at a state $\Phi = \Phi_0$ if at that state, the eigenvalues of the flux Jacobian

$$\mathcal{J}_\mathbf{f}(\Phi) := (\partial f_i / \partial \phi_j)_{1 \leq i, j \leq N}$$

are all real, and *strictly hyperbolic* if these are, moreover, pairwise distinct. For polydisperse sedimentation models, a particular result of the hyperbolicity analysis states that under determined conditions the eigenvalues of $\mathcal{J}_\mathbf{f}(\Phi)$, which are inaccessible in closed form, interlace with the given phase velocities v_i . This interlacing property is the basis of characteristic-wise (spectral, as opposed to component-wise) high-resolution numerical schemes for the approximation of discontinuous solutions of (BSM) (see [18]). It is particularly important to note that spectral weighted essentially non-oscillatory schemes (WENO schemes; see [35, 39, 48, 53]) are more accurate, and mostly more efficient, than their (easier to implement) component-wise (COMP) counterparts. Substantial further improvements of efficiency are possible by adaptive techniques, for instance Adaptive Mesh Refinement (AMR) [23].

In the context of polydisperse sedimentation, the hyperbolicity of (2.1) is related to the stability of the separation of a polydisperse mixture, as is detailed in [8, 21]. Roughly speaking, stability in this context means that an initially homogeneous mixture of a given initial composition Φ_0 segregates under the formation of horizontal discontinuities and vertical gradients, and that blobs, fingers, and other structures related to instable separation do not occur. A linear stability analysis applied to (2.1) reveals that these phenomena are not amplified when $\mathcal{J}_\mathbf{f}(\Phi_0)$ has real eigenvalues only, that is (2.1) is hyperbolic at Φ_0 . Since on the other hand, instabilities such as blobs and fingers have been observed for bidisperse mixtures ($N = 2$) only when particles with different densities are involved ($\rho_1 \neq \rho_2$), one should expect that a sound mathematical model should be hyperbolic for equal-density particles, arbitrary N and $\delta_N \ll 1$. This was proved in [11] for the MLB model (precisely, for the version (1.5), (BSM)).

2.1 Secular equation and interlacing property

In many cases, one may exploit the systematic algebraic construction of the velocity functions v_i for the hyperbolicity analysis as follows. Many models (proposed choices of $v_i(\Phi)$) can be written as

$$v_i = v_i(p_1, \dots, p_m), \quad p_l = p_l(\Phi), \quad m \ll N,$$

i.e., the velocity v_i of species i does not depend on each of the N components ϕ_1, \dots, ϕ_N of Φ individually, but rather on a small number $m \ll N$ of functions $p_1(\Phi), \dots, p_m(\Phi)$. One then obtains that $\mathcal{J}_\mathbf{f}(\Phi)$ is a rank- m perturbation of the diagonal matrix $\mathbf{D} := \text{diag}(v_1, \dots, v_N)$. Precisely, one can write

$$\mathcal{J}_\mathbf{f} = \mathbf{D} + \mathbf{B}\mathbf{A}^T, \quad \begin{cases} \mathbf{B} := (B_{il}) = (\phi_i \partial v_i / \partial p_l), & 1 \leq i, j \leq N, \\ \mathbf{A} := (A_{jl}) = (\partial p_l / \partial \phi_j), & 1 \leq l \leq m. \end{cases}$$

The following theorem indicates how this structure can be exploited to facilitate the location of eigenvalues.

Theorem 2.1 (The secular equation [3]). *A number $\lambda \notin \{v_1, \dots, v_N\}$ is an eigenvalue of the matrix $\mathbf{D} + \mathbf{B}\mathbf{A}^T$ if and only if $R(\lambda) = 0$ (the “secular equation”), where we define*

$$R(\lambda) := \det [\mathbf{I} + \mathbf{A}^T (\mathbf{D} - \lambda \mathbf{I})^{-1} \mathbf{B}] = 1 + \sum_{i=1}^N \frac{\gamma_i}{v_i - \lambda}, \quad \gamma_i := \sum_{r=1}^{\min\{N, m\}} \sum_{I \in S_r^N, J \in S_r^m} \frac{\det \mathbf{A}^{I,J} \det \mathbf{B}^{I,J}}{\prod_{l \in I, l \neq i} (v_l - v_i)},$$

where S_r^N is the set of all subsets of $\{1, \dots, N\}$ with r elements, and S_r^m is defined analogously.

From Theorem 2.1 one may deduce the following result.

Corollary (Interlacing property). *If $\gamma_i \cdot \gamma_j > 0$ for all i, j , then $\mathbf{D} + \mathbf{B}\mathbf{A}^T$ is diagonalizable with real eigenvalues $\lambda_1, \dots, \lambda_N$. Let $\tilde{\gamma} := \sum_{i=1}^N \gamma_i$. Then*

$$\begin{aligned} M_1 &:= v_N + \tilde{\gamma} < \lambda_N < v_N < \lambda_{N-1} < \dots < \lambda_1 < v_1, \\ v_N < \lambda_N < v_{N-1} < \lambda_{N-1} < \dots < v_1 < \lambda_1 &< M_2 := v_1 + \tilde{\gamma}. \end{aligned}$$

One may easily verify that the MLB model for equal-density particles, as described by (1.5), is a case of $m = 2$ with $\gamma_i < 0$ follows easily; thus, in this case (BSM) is strictly hyperbolic for all $\Phi > 0$. The eigenvalues satisfy the interlacing property. On the other hand, for the models by Batchelor and Wen [9], Davis and Gecol [27] and others one can prove definite sign of γ_i only if $\delta_N > \delta_{\min, \text{model}}(\delta, \phi_{\max}) > 0$, that is for a finite range of particle size ratios. For a given eigenvalue $\lambda \notin \{v_1, \dots, v_N\}$, the eigenvectors can be calculated efficiently when the interlacing property is in effect.

2.2 SPEC-INT and COMP-GLF numerical schemes

We now consider the numerical approximation of discontinuous solutions of (BSM). A conservative, fully discrete scheme for the computation of $\Phi_i^n \approx \Phi(x_i = (i + \frac{1}{2})\Delta x, t_n = n\Delta t)$ can be written as

$$\begin{aligned} \Phi_i^{n+1} &= \Phi_i^n - \frac{\Delta t}{\Delta x} (\hat{\mathbf{f}}_{i+1/2} - \hat{\mathbf{f}}_{i-1/2}), \\ \hat{\mathbf{f}}_{i+1/2} &= \hat{\mathbf{f}}(\Phi_{i-s+1}^n, \dots, \Phi_{i+s}^n), \quad i = 0, \dots, M-1; \quad \hat{\mathbf{f}}_{-1/2} = \hat{\mathbf{f}}_{M-1/2} = \mathbf{0}, \end{aligned}$$

where $\hat{\mathbf{f}}_{i+1/2}$ is the numerical flux vector associated with the cell interface x_{i+1} . In general, the basic idea of construction of numerical schemes consists in applying an ODE solver (in our case, a third-order Kunge-Kutta TVD method) to the spatially semi-discretized equations [49].

To compute $\hat{\mathbf{f}}_{i+1/2}$, one may use the eigenstructure of $\mathcal{J}_{\mathbf{f}}(\Phi_{i+1/2})$, where $\Phi_{i+1/2} := \frac{1}{2}(\Phi_i + \Phi_{i+1})$, given by the right and left eigenvectors:

$$\mathbf{R}_{i+1/2} = [\mathbf{r}_{i+1/2,1}, \dots, \mathbf{r}_{i+1/2,N}], \quad (\mathbf{R}_{i+1/2}^{-1})^T = [\mathbf{l}_{i+1/2,1}, \dots, \mathbf{l}_{i+1/2,N}].$$

From a local flux splitting

$$\mathbf{f}^{-k} + \mathbf{f}^{+,k} = \mathbf{f}, \quad \pm \lambda_k(\mathcal{J}_{\mathbf{f}^{\pm k}}(\Phi)) \geq 0, \quad \Phi \approx \Phi_{i+1/2}, \quad k = 1, \dots, N,$$

we can define $g_j^{\pm k} := \mathbf{l}_{i+1/2,k}^T \cdot \mathbf{f}^{\pm k}(\Phi_j)$, and use upwind-biased reconstructions \mathcal{R}^\pm (e.g., the WENO method), to calculate

$$\begin{aligned} \hat{g}_{i+1/2,k} &= \mathcal{R}^+(\mathbf{g}_{i-s+1}^{+,k}, \dots, \mathbf{g}_{i+s-1}^{+,k}; x_{i+1/2}) + \mathcal{R}^-(\mathbf{g}_{i-s+2}^{-,k}, \dots, \mathbf{g}_{i-s}^{-,k}; x_{i+1/2}), \\ \hat{\mathbf{f}}_{i+1/2} &= \mathbf{R}_{i+1/2} \hat{\mathbf{g}}_{i+1/2} = \sum_{k=1}^n \hat{g}_{i+1/2,k} \mathbf{r}_{i+1/2,k}. \end{aligned}$$

The component-wise global Lax-Friedrichs (COMP-GLF) scheme is based on the alternative of setting $\mathbf{R}_{i+1/2} = \mathbf{I}_N$, where \mathbf{I}_N is the $N \times N$ identity matrix, and utilizing a global flux splitting $\mathbf{f}^- + \mathbf{f}^+ = \mathbf{f}$, where $\pm \lambda_k(\mathcal{J}_{\mathbf{f}^\pm}(\Phi)) \geq 0$ for all k . This results in the choice

$$g_j^{\pm k} = \mathbf{e}_k^T \mathbf{f}^\pm(\Phi_j) = f_k^\pm(\Phi_j),$$

which leads to a high-order extension of the Lax-Friedrichs scheme.

A more sophisticated scheme is based on spectral properties of the flux Jacobian in conjunction with the interlacing property (Corollary 2.1), to which we refer as SPEC-INT scheme. To outline it, we assume that $\mathcal{S}_{i+1/2}$ is the segment joining states Φ_i and Φ_{i+1} . If $\lambda_k(\mathcal{J}_{\mathbf{f}}(\Phi)) > 0$ (resp., < 0) on $\mathcal{S}_{i+1/2}$ then we

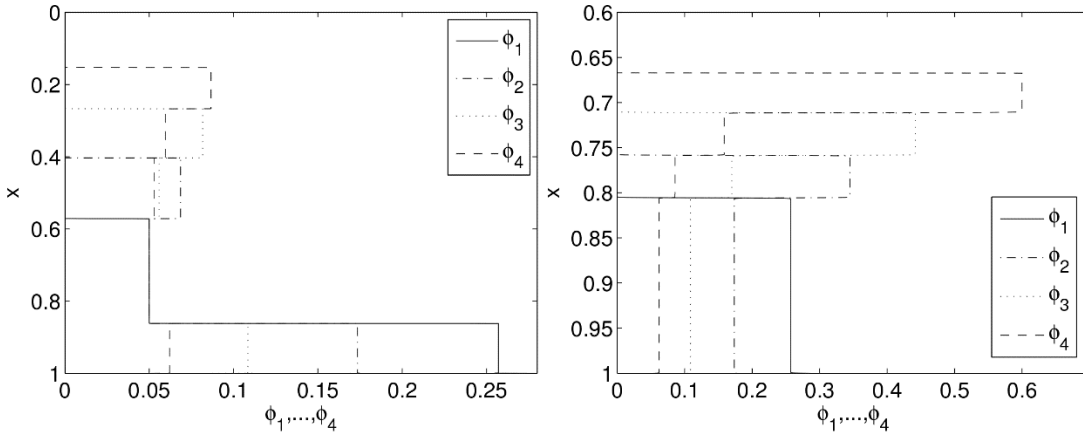


Fig. 2: Example 1 (settling of a suspension of $N = 4$ solid species): reference solution with $M = M_{\text{ref}} = 6400$ at simulated times $t = 50$ s and $t = 300$ s [18].

upwind (no need for flux splitting). However, if $\lambda_k(\mathcal{J}_f(\Phi))$ changes sign on $\mathcal{S}_{i+1/2}$, then we use a local Lax-Friedrichs flux splitting with numerical viscosity parameter α_k :

$$\mathbf{f}^{\pm,k}(\Phi) = \mathbf{f}(\Phi) \pm \alpha_k \Phi, \quad \alpha_k \geq \max_{\Phi \in \mathcal{S}_{i+1/2}} |\lambda_k(\mathcal{J}_f(\Phi))|.$$

The computation of this parameter depends decisively on the result of Corollary 2.1. While by preliminary tests it had turned out that the amount of numerical viscosity is insufficient for the usual choice

$$\alpha_k = \max\{|\lambda_k(\mathcal{J}_f(\Phi_i))|, |\lambda_k(\mathcal{J}_f(\Phi_{i+1}))|\},$$

much better results in terms of resolution and efficiency have been obtained by exploiting the interlacing property stated in the corollary. For example, for the MLB model with equal-density particles the interlacing property provides the easily computable bound

$$\max_{\Phi \in \mathcal{S}_{i+1/2}} |\lambda_k(\Phi)| \leq \alpha_k := \max \left\{ \max_{\Phi \in \mathcal{S}_{i+1/2}} |v_k(\Phi)|, \max_{\Phi \in \mathcal{S}_{i+1/2}} |v_{k+1}(\Phi)| \right\}.$$

This choice of $\alpha_1, \dots, \alpha_N$ defines the scheme SPEC-INT.

2.3 Numerical experiments

We here present some selected numerical examples from [18] and [23]. We refer to these papers for a detailed presentation and broader discussion. In Example 1, we consider a suspension of $N = 4$ equal-density particle species with the normalized sizes $d_1 = 1$, $d_2 = 0.8$, $d_3 = 0.6$, and $d_4 = 0.4$, and set $\phi_{\max} = 0.6$. The initial composition is $\phi_i^0 = 0.05$ for $i = 1, \dots, 4$. Numerical results are shown in Figures 2 and 3.

Example 2 is motivated by data from [31] and concerns the settling of a suspension with $N = 7$ solid species (size classes). We consider the parameters $\phi_{\max} = 0.6$ and the hindered settling factor $V(\phi) = (1 - \phi)^3$. The initial conditions ϕ_i^0 , real particle sizes d_i , and normalized squared particle sizes δ_i are given here:

i	1	2	3	4	5	6	7
$\phi_i^0[10^{-2}]$	0.2365	1.1039	3.5668	3.8776	6.0436	10.890	4.2718
$d_i [10^{-5} \text{ m}]$	290	250	210	170	130	90	50
δ_i	1.0000	0.7432	0.5244	0.3436	0.2010	0.0963	0.0297

We use Adaptive Mesh Refinement (AMR) to locally enhance resolution and efficiency. The final scheme is named SPEC-INT-AMR. Numerical results from [23] are shown in Figures 4 and 5.

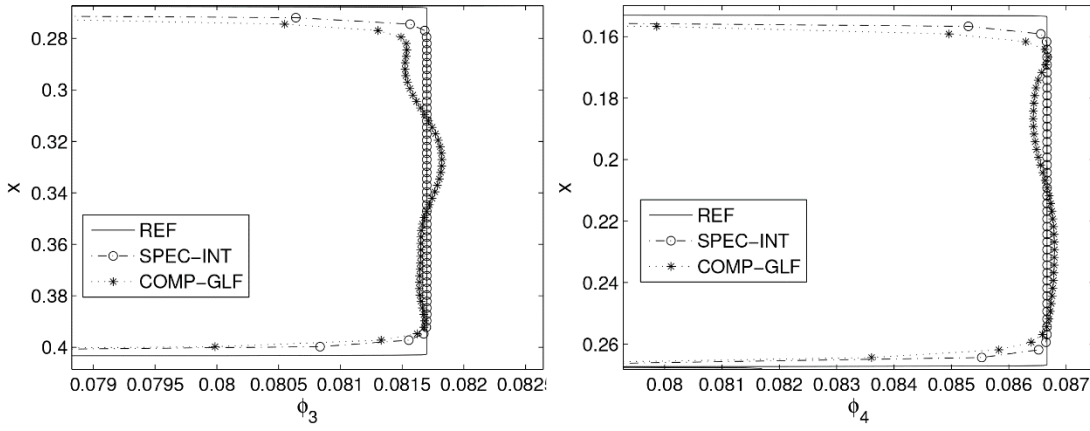


Fig. 3: Example 1 (settling of a suspension of $N = 4$ solid species): solution for ϕ_3 and ϕ_4 with $M = 400$ at simulated time $t = 50$ s [18].

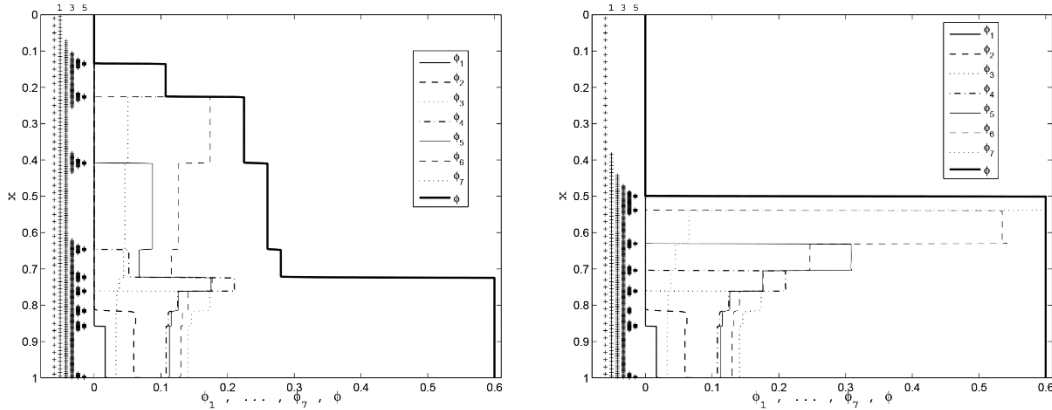


Fig. 4: Example 2 (settling of a suspension of $N = 7$ solid species): numerical solutionx at $t = 400$ s and $t = 2500$ s obtained by SPEC-INT-AMR with $L + 1 = 6$ levels; the coarsest grid has 50 subintervals [23].

3 Implicit-explicit (IMEX) methods for a diffusively corrected model

The diffusively corrected model (including the effect of sediment compressibility) leads to a strongly degenerate hyperbolic-parabolic system of PDEs (DCM). Explicit schemes applied to the model require the strong stability step size constraint

$$\alpha \frac{\Delta t}{\Delta x} + \beta \frac{\Delta t}{\Delta x^2} \leq 1,$$

which is avoided by so-called implicit-explicit Runge-Kutta (IMEX-RK) discretizations that are implicit for diffusive term and explicit for the convective term, both of the semi-discrete (spatially discretized) formulation. In [24] the authors developed a new nonlinear solver for the regularization of the algebraic systems arising with IMEX methods. Alternatively, one can design linearly implicit (less accurate, but easier to implement) IMEX-RK schemes to solve the problem [13, 14].

3.1 Spatial discretization

The spatial discretization of (DCM) is achieved through discretizing $\partial_x f(\Phi)$ discretized by $\frac{1}{\Delta x}(\Delta^- f)(\Phi)$, where the numerical flux is a fifth-order WENO reconstructions of characteristic fluxes (WENO-SPEC or

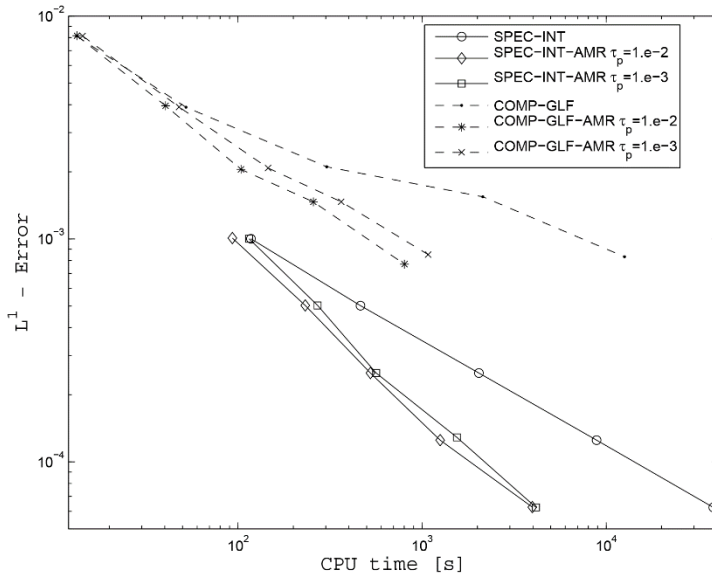


Fig. 5: Example 2 (settling of a suspension of $N = 7$ solid species): approximate L^1 errors versus CPU time for SPEC-INT-AMR and COMP-GLF-AMR at $t = 2500$ s. The referee solution was computed with SPEC-INT on a fixed grid with 12800 subintervals [23].

SPEC-INT, see Section 2.2 and [18]). Moreover, $\partial_x(\mathbf{B}(\Phi)\partial_x\Phi)$ is discretized by a standard second-order scheme, i.e.,

$$\begin{aligned}\partial_x(\mathbf{B}(\Phi)\partial_x\Phi)(x_i, t) &\approx \frac{1}{\Delta x^2} (\mathbf{B}_{i-1/2}\Phi_{i-1} - (\mathbf{B}_{i-1/2} + \mathbf{B}_{i+1/2})\Phi_i + \mathbf{B}_{i+1/2}\Phi_{i+1})(t), \\ \mathbf{B}_{i+1/2} &:= \frac{1}{2}(\mathbf{B}(\Phi_i) + \mathbf{B}(\Phi_{i+1})), \quad \Phi_i(t) \approx \Phi(x_i, t) \in \mathbb{R}^N;\end{aligned}$$

Modifications to these formulas apply for $i = 1$ and $i = M$ to account for boundary conditions. BCs. For $\Phi = (\Phi_1, \dots, \Phi_M)^T \in \mathbb{R}^{MN}$, we can now define the $M \times M$ block tridiagonal matrix $\mathcal{B} = \mathcal{B}(\Phi)$, with blocks of size $N \times N$, as $\mathcal{B}_{i,i} = -(\mathbf{B}_{i-1/2} + \mathbf{B}_{i+1/2})$, $\mathcal{B}_{i,i-1} = \mathbf{B}_{i-1/2}$, etc.

3.2 Time discretization

Within Semi-implicit IMEX-RK schemes, the convective term is treated explicitly, and the diffusive term is treated implicitly. One combines explicit Runge-Kutta (ERK) scheme with a diagonally implicit Runge-Kutta (DIRK) scheme to handle the former and the latter, respectively. Both schemes are assumed to be given by the usual Butcher arrays, that is

$$\frac{\tilde{c}}{\tilde{\mathbf{B}}^T} = s\text{-stage ERK}, \quad \frac{c}{\mathbf{B}^T} = s\text{-stage DIRK}.$$

A common example is the second-order scheme IMEX-SSP2(3,3,2) (see [34]):

$$\frac{\tilde{c}}{\tilde{\mathbf{B}}^T} = \frac{0}{\frac{1}{2}} \left| \begin{array}{ccc} 0 & 0 & 0 \\ \frac{1}{2} & 0 & 0 \\ 1 & \frac{1}{2} & \frac{1}{2} \end{array} \right|, \quad \frac{c}{\mathbf{B}^T} = \frac{\frac{1}{4}}{1} \left| \begin{array}{ccc} \frac{1}{4} & 0 & 0 \\ 0 & \frac{1}{4} & 0 \\ \frac{1}{3} & \frac{1}{3} & \frac{1}{3} \end{array} \right|.$$

Nonlinearly implicit IMEX-RK (NI-IMEX-RK) methods (as studied in [24]) are based on the semidiscrete formulation rewritten as follows:

$$\begin{aligned}\frac{d\Phi}{dt} &= C(\Phi) + D(\Phi), \\ C(\Phi) &:= -\frac{1}{\Delta x}(\Delta^- f)(\Phi), \quad D(\Phi) := \frac{1}{\Delta x^2}\mathcal{B}(\Phi)\Phi,\end{aligned}$$

where $C(\Phi)$ and $D(\Phi)$ represent the spatial discretizations of the convective and diffusive parts of (DCM), respectively. For this setting the simplest IMEX scheme is

$$\Phi^{n+1} = \Phi^n - \frac{\Delta t}{\Delta x}(\Delta^- f)(\Phi^n) + \frac{\Delta t}{\Delta x^2}\mathcal{B}(\Phi^{n+1})\Phi^{n+1},$$

where $\Phi^n \approx \Phi(t^n)$. For general pairs of RK schemes, the computations of a NI-IMEX-RK scheme necessary to advance an Φ^n from time t^n to $t^{n+1} = t^n + \Delta t$ are given in the following algorithm:

Input: approximate solution vector Φ^n for $t = t_n$

do $i = 1, \dots, s$

solve for $\Phi^{(i)}$ the nonlinear equation

$$\Phi^{(i)} = \Phi^n + \Delta t \left(\sum_{j=1}^{i-1} a_{ij} K_j + a_{ii} D(\Phi^{(i)}) + \sum_{j=1}^{i-1} \tilde{a}_{ij} \tilde{K}_j \right)$$

$$K_i \leftarrow D(\Phi^{(i)}), \tilde{K}_i \leftarrow C(\Phi^{(i)})$$

enddo

$$\Phi^{n+1} \leftarrow \Phi^n + \Delta t \sum_{j=1}^s b_j K_j + \Delta t \sum_{j=1}^s \tilde{b}_j \tilde{K}_j$$

Output: approximate solution vector Φ^{n+1} for $t = t^{n+1} = t^n + \Delta t$.

This algorithm [4] requires in each step solving a nonlinear system of the type

$$\Psi_i(\mathbf{u}) := \mathbf{u} - a_{ii}\Delta t D(\mathbf{u}) - \mathbf{r}_i = 0, \quad i = 1, \dots, s, \quad (3.1)$$

for $\mathbf{u} = \Phi^{(i)} \in \mathbb{R}^{MN}$, where

$$\mathbf{r}_i = \Phi^n + \Delta t \left(\sum_{j=1}^{i-1} a_{ij} K_j + \sum_{j=1}^{i-1} \tilde{a}_{ij} \tilde{K}_j \right).$$

To apply the standard Newton-Raphson iterative method, one must require that the function \mathbf{B} or \mathcal{B} is at least of class C^1 . However, our degenerate model does not naturally satisfy this assumption. To this end, we devised NI-IMEX-RK schemes [24] that are based on replacing \mathbf{B} by smooth approximation \mathbf{B}_ε (and \mathcal{B} by \mathcal{B}_ε), where $\mathbf{B}_\varepsilon \rightarrow \mathbf{B}$ and $\mathcal{B}_\varepsilon \rightarrow \mathcal{B}$ as $\varepsilon \rightarrow 0$. One then applies a nonlinear solver combined with smoothing and a damped Newton-Raphson method with line search strategy (see [24] for details).

The necessity to solve nonlinear algebraic systems within each IMEX step circumvented by linearly implicit Runge-Kutta methods (LI-IMEX-RK methods). To formulate them, we start from the semidiscrete formulation in the form

$$\begin{aligned}\frac{d\Phi}{dt} &= \mathcal{C}(\Phi) + \mathcal{D}(\Phi, \Phi), \\ \mathcal{C}(\Phi) &:= -\frac{1}{\Delta x}(\Delta^- f)(\Phi), \quad \mathcal{D}(\Phi^*, \Phi) := \frac{1}{\Delta x^2}\mathcal{B}(\Phi^*)\Phi,\end{aligned}$$

where we distinguish between stiff and nonstiff dependence on Φ in the spatially discretized form $\mathcal{D}(\Phi^*, \Phi)$ of the diffusion term. We write

$$\frac{d\Phi}{dt} = \mathcal{C}(\Phi^*) + \mathcal{D}(\Phi^*, \Phi) =: \mathcal{K}(\Phi^*, \Phi),$$

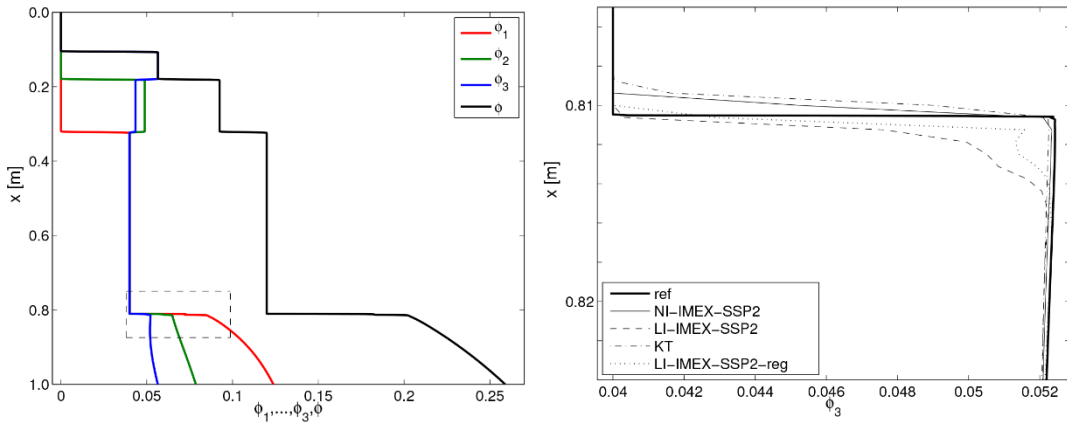


Fig. 6: Example 3 (settling of a tridisperse suspension ($N = 3$), including the effect of sediment compressibility): (left) numerical results by LI-IMEX-SSP2 at simulated time $T = 4000$ s, (right) enlarged view [13, 14].

where Φ^* is treated explicitly as argument of f and \mathcal{B} , while Φ is implicit in the term to which \mathcal{B} is applied. The simplest first-order LI-IMEX-RK scheme is then given by

$$\Phi^{n+1} = \Phi^n - \frac{\Delta t}{\Delta x} (\Delta^- f)(\Phi^n) + \frac{\Delta t}{\Delta x^2} \mathcal{B}(\Phi^n) \Phi^{n+1}.$$

In the general case, a linearly implicit IMEX-RK scheme is defined by the following algorithm:

```

Input: approximate solution vector  $\Phi^n$  for  $t = t^n$ 

do  $i = 1, \dots, s$ 
     $\Phi^{*(i)} \leftarrow \Phi^n + \Delta t \sum_{j=1}^{i-1} \tilde{a}_{ij} K_j, \quad \hat{\Phi}^{(i)} \leftarrow \Phi^n + \Delta t \sum_{j=1}^{i-1} a_{ij} K_j$ 
    solve for  $K_i$  the linear equation
    
$$K_i = \mathcal{C}(\Phi^{*(i)}) + \frac{1}{\Delta t^2} \mathcal{B}(\Phi^{*(i)}) (\hat{\Phi}^{(i)} + \Delta t a_{ii} K_i), \quad (*)$$

enddo


$$\Phi^{n+1} \leftarrow \Phi^n + \Delta t \sum_{j=1}^s b_j K_j \quad (**)$$


```

Output: approximate solution vector Φ^{n+1} for $t = t^{n+1} = t^n + \Delta t$.

The property $\Phi^{*,n+1} = \Phi^{n+1}$ is guaranteed for $b_i = \tilde{b}_i$ for $i = 1, \dots, s$ [15].

3.3 Numerical experiments

We compare numerical results with those obtained from the well-known explicit Kurganov-Tadmor (KT) scheme [37]. We set $\Delta x = L/M$ and in each iteration, the time step Δt is determined by

$$\frac{\Delta t}{\Delta x} \max_{1 \leq j \leq M} \rho(\mathcal{J}_f(\Phi_j^n)) + \frac{\Delta t}{2\Delta x^2} \max_{1 \leq j \leq M} \rho(\mathbf{B}(\Phi_j^n)) = C_{\text{cfl}_1}$$

for the KT scheme and

$$\frac{\Delta t}{\Delta x} \max_{1 \leq j \leq M} \rho(\mathcal{J}_f(\Phi_j^n)) = C_{\text{cfl}_2}$$

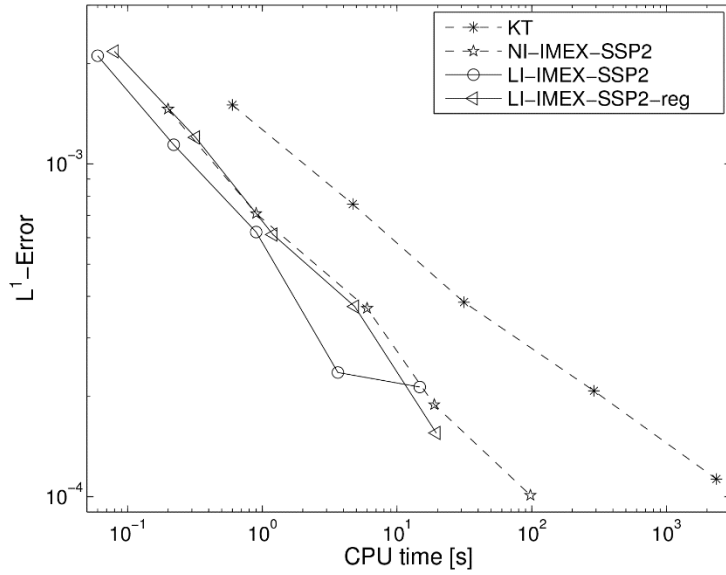


Fig. 7: Example 3 (settling of a tridisperse suspension ($N = 3$), including the effect of sediment compressibility): numerical solution at simulated time $T = 4000$ s, efficiency plot based on numerical results for $\Delta x = 1/M$ with $M = 100, 200, 400, 800$ and 1600 [13, 14].

for the semi-implicit schemes, where $\rho(\cdot)$ is the spectral radius. In the numerical examples we choose C_{cfl_*} as the largest multiple of 0.05 that yields oscillation-free numerical solutions. In all cases, the reference solution for numerical tests is computed by the KT scheme with $M_{\text{ref}} = 25600$. The numerical examples are based on the results of [13, 14].

In Example 3 we consider $N = 3$ and focus on the comparison of LI- and NI-IMEX-SSP2 schemes, based on using the model parameters $\phi_{\max} = 0.66$, $n_{RZ} = 4.7$, $\sigma_0 = 180 \text{ Pa}$, $\phi_c = 0.2$, $k = 2$, $\mu_f = 10^{-3} \text{ Pas}$, $d = 1.19 \times 10^{-5} \text{ m}$, $\bar{\rho}_s = 1800 \text{ kg/m}^3$, and $g = 9.81 \text{ m/s}^2$. The initial concentration is $\Phi_0 = (0.04, 0.04, 0.04)^T$ in a vessel of height $\mathcal{L} = 1 \text{ m}$ with $\delta = (1, 0.5, 0.25)^T$. For the nonlinearly implicit scheme, NI-IMEX-SSP2, the regularization is achieved by utilizing

$$\sigma_e(\phi; \varepsilon) = \sigma_e(\phi) \exp(-\varepsilon/(\phi - \phi_c)^2), \quad \varepsilon > 0,$$

where ε decreases gradually from $\varepsilon_0 = 10^{-4}$ to $\varepsilon_{\min} = 10^{-6}$, $\text{tol} = 10^{-8}$. The schemes LI-IMEX-SSP2 and KT do not include regularization of the diffusive term. For the schemes NI-IMEX-SSP2 and LI-IMEX-SSP2, we set $C_{\text{cfl}_2} = 0.7$, and for KT, $C_{\text{cfl}_1} = 0.25$. The scheme LI-IMEX-SSP2-reg consists in applying the scheme LI-IMEX-SSP2 to the regularized diffusion term with $\varepsilon_{\min} = 10^{-6}$.

In Example 4 we again consider $N = 3$ and the parameters $d_1 = 1.0$, $d_2 = 0.8$ and $d_3 = 0.7$, with a smooth initial concentration profile $\phi_i(x) = 0.12 \exp(-200(x - 0.5)^2)$. The numerical results produced by the scheme LI-IMEX-SSP2-reg with $M = 1600$ are taken at $T = 20$ s (when the solution profiles are still smooths) and $T = 500$ s (after discontinuities have formed). The corresponding numerical errors are given here [13]:

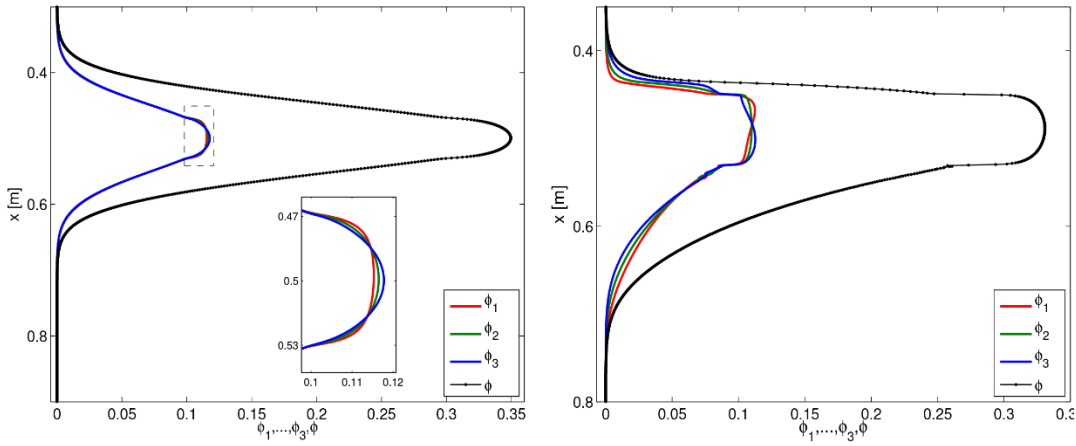


Fig. 8: Example 4: (settling of a tridisperse suspension ($N = 3$), including the effect of sediment compressibility, smooth initial datum): numerical results produced by LI-IMEX-SSP2-reg with $M = 1600$ at simulated times (left) $T = 20\text{s}$ and (right) $T = 500\text{s}$ [13].

M	$T = 20\text{s}$				$T = 500\text{s}$	
	based on reference soln. $e_M^{\text{tot}}(T)$	$\theta_M(T)$	based on interpolation $\hat{\theta}_M(T)$	$\tilde{e}_M^{\text{tot}}(T)$	based on reference soln. $e_M^{\text{tot}}(T)$	$\theta_M(T)$
50	1.38e-04	0.14	-0.33	8.41e-05	2.27e-03	1.59
100	1.25e-04	1.45	1.48	1.06e-04	7.49e-04	0.95
200	4.58e-05	1.80	1.68	3.80e-05	3.86e-04	1.11
400	1.30e-05	1.88	1.76	1.19e-05	1.78e-04	0.91
800	3.54e-06	1.87	1.87	3.52e-06	9.49e-05	1.05
1600	9.66e-07	2.00	1.98	9.63e-07	4.56e-05	1.01
3200	2.40e-07	2.06	—	2.44e-07	2.26e-05	1.01
6400	5.73e-08	—	—	—	1.12e-05	—

4 A multilayer shallow water system of polydisperse sedimentation

4.1 Model formulation

Models for the settling of a polydisperse suspensions in two or three space dimensions are usually given by (1.1)–(1.3) or a similar coupled transport-flow problem. Roughly speaking, such problems are defined by a transport equation (for the solids concentrations) strongly coupled to a version of the Navier-Stokes equation for the mixture velocity and the pressure. Since the computational effort to solve these multi-dimensional coupled problems is considerable, one seeks to define easier-to-solve lower-dimensional models. The well-known Saint-Venant (shallow water) approach is based on a vertically integrated version of the flow equations that can be applied when vertical fluctuations of variables are negligible.

To handle mostly horizontal flows combined with polydisperse sedimentation, a new computational multilayer Saint-Venant approach was developed [32] and recently modified [20]. In general, a multilayer Saint-Venant model is less expensive than the full 3D model from the computational point of view, but still keeps information on the vertical distribution of the mixture. Such an approach (as opposed to a standard single-layer approach) is appropriate in the presence large friction coefficients, significant water depth, or wind effects [6, 7, 44]. This approach results in a number of coupled Saint-Venant system, one for each layer [5], see Figure 9.

The steps of the formulation of the final solvable multiplayer model are fairly complicated [32]. They include integrating the balance equations for the solid and liquid phases over each layer, neglecting vertical

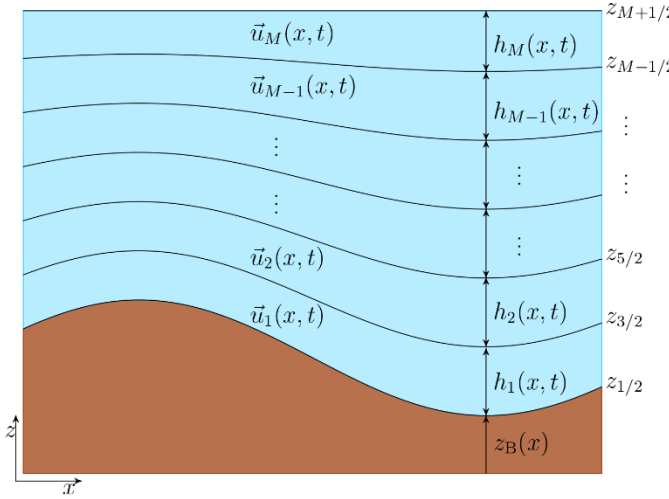


Fig. 9: Multilayer approach for one horizontal and one vertical space dimension (coordinates x and z , respectively) [20].

fluctuations of horizontal velocities and concentrations inside each layer, and assuming that the pressure is hydrostatic. We assume that the suspension body is subdivided into M layers. Furthermore, if $h = h(x, t)$ denotes the total height of the suspension body at horizontal position x at time t , then we assume that the height of layer α , $\alpha = 1, \dots, M$, is a fixed fraction l_α of h , such that $h_\alpha = l_\alpha h$ for $l_\alpha > 0$, $\alpha = 1, \dots, M$, with $l_1 + \dots + l_M = 1$. We assume that the bottom and surface heights are $z_B := z_{1/2}$ and $z_S := z_{M+1/2}$, such that $h = z_S - z_B = h_1 + \dots + h_M$. (again, see Figure 9). The governing model can then be written as follows, where $\alpha = 1, \dots, M$ counts the layer under consideration and $j = 1, \dots, N$ indicates the solid particle species:

$$\begin{aligned}
& \partial_t r_{j,\alpha} + \partial_x \left(\frac{r_{j,\alpha} q_\alpha}{m_\alpha} \right) \\
&= \frac{1}{l_\alpha} (\tilde{\phi}_{j,\alpha+1/2} G_{\alpha+1/2} - \tilde{\phi}_{j,\alpha-1/2} G_{\alpha-1/2}) - \frac{\rho_j}{l_\alpha} (\tilde{f}_{j,\alpha+1/2} - \tilde{f}_{j,\alpha-1/2}), \quad j = 1, \dots, N, \\
& \partial_t q_\alpha + \partial_x \left(\frac{q_\alpha^2}{m_\alpha} + h \left(p_s + \frac{g}{2} l_\alpha m_\alpha + g \sum_{\beta=\alpha+1}^M l_\beta m_\beta \right) \right) \\
&= \left(p_s + g \sum_{\beta=\alpha+1}^M l_\beta m_\beta \right) \partial_x h - g m_\alpha \partial_x z_b - g m_\alpha l_{\alpha-1} \partial_x h + \frac{1}{l_\alpha} (\tilde{u}_{\alpha+1/2} G_{\alpha+1/2} - \tilde{u}_{\alpha-1/2} G_{\alpha-1/2}), \\
& \partial_t \bar{m} + \partial_x \left(\sum_{\beta=1}^M l_\beta q_\beta \right) = G_{M+1/2} - G_{1/2}, \quad \bar{m} := h \sum_{\beta=1}^M \bar{\rho}_\beta l_\beta = \sum_{\beta=1}^M l_\beta m_\beta.
\end{aligned} \tag{4.1}$$

Here ρ_1, \dots, ρ_N are the densities of the solid species, ρ_0 is the density of the fluid, g is the acceleration of gravity, $\phi_{j,\alpha}$ denotes the volume fraction of species j in layer α , $r_{j,\alpha} := \rho_j \phi_{j,\alpha} h$, u_α is the horizontal velocity of the mixture in layer α , $\bar{\rho}_\alpha := \rho_0 \phi_{0,\alpha} + \rho_1 \phi_{1,\alpha} + \dots + \rho_N \phi_{N,\alpha}$ is the density of layer α , $q_\alpha := \bar{\rho}_\alpha h u_\alpha$, and $m_\alpha := \bar{\rho}_\alpha h$. Moreover,

$$\tilde{u}_{\alpha+1/2} := \frac{1}{2} \left(\frac{q_{\alpha+1}}{m_{\alpha+1}} + \frac{q_\alpha}{m_\alpha} \right), \quad \tilde{\phi}_{j,\alpha+1/2} := \frac{1}{2} \left(\frac{r_{j,\alpha+1}}{m_{\alpha+1}} + \frac{r_{j,\alpha}}{m_\alpha} \right),$$

and $G_{j,\alpha+1/2}$ are intra-layer mass fluxes defined inter alia by the modified MLB velocities. The model that is eventually solved can be written as a balance equation involving non-conservative products,

$$\begin{aligned}
& \partial_t \mathbf{w} + \partial_x \mathcal{F}(\mathbf{w}) = \mathcal{S}(\mathbf{w}, \partial_x \mathbf{w}) + \mathcal{G}(\mathbf{w}, \partial_x \mathbf{w}), \\
& \mathbf{w} = (\bar{m}, q_1, \dots, q_M, r_{1,1}, \dots, r_{N,1}, \dots, r_{1,M}, \dots, r_{N,M})^T,
\end{aligned}$$

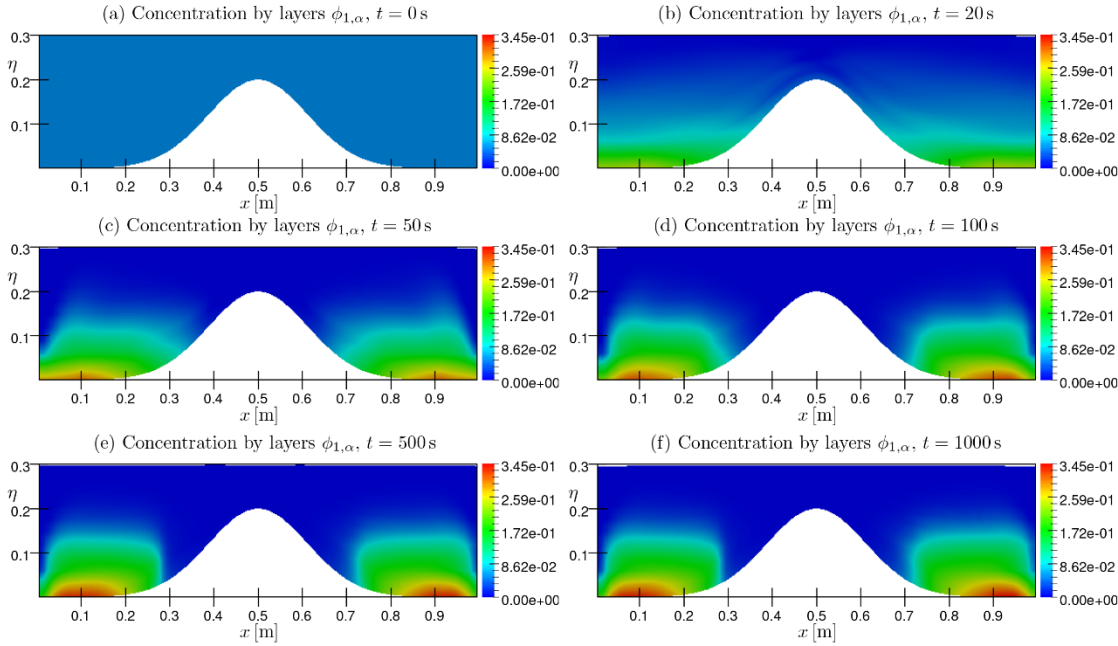


Fig. 10: Example 5: Concentration of ϕ_1 by color in a domain with a bump, $\eta(x) = z_B(x) + h(x)$ m, at simulated times $T = 0$ s, 20 s, 50 s, 100 s, 500 s and $T = 1000$ s.

for whose numerical solution specialized numerical methods are available.

4.2 Numerical experiments

In the present numerical simulation we have used the global constants $g = 9.8 \text{ m/s}^2$ (acceleration of gravity), $\phi_{\max} = 0.68$, and we have employed the Richardson-Zaki hindered settling factor with $n_{RZ} = 4.7$, viscosity and density of the pure fluid are $\mu_0 = 0.02416 \text{ Pas}$ and $\rho_0 = 1208 \text{ kg/m}^3$, respectively, and we are assumed that the all species have the same density $\rho_1 = \rho_2 = \rho_3 = 2790 \text{ kg/m}^3$.

The (horizontal) x -interval $[0, L]$ has been discretized into C subintervals $[x_{i-1/2}, x_{i+1/2}] = [(i-1)\Delta x, i\Delta x]$ of length $\Delta x = L/C$, centered at $x_i = (i - 1/2)\Delta x$, $i = 1, \dots, C$, and in the vertical direction we have used $M = 10$ layers. Finally, we use

$$\frac{\Delta t}{\Delta x} \max_{1 \leq i \leq C} \max\{|S_{R,i+1/2}|, |S_{L,i+1/2}|\} = C_{\text{cfl}},$$

as C_{cfl} condition, where $S_{R,i+1/2}$ and $S_{L,i+1/2}$ are the bounds of the eigenvalues. Here we have considered $C_{\text{cfl}} = 0.5$.

In this numerical test we simulate polidisperse sedimentation process over a horizontal channel with a bump of length $L = 1$ m. We use $N = 3$ solids species dispersed in a viscous fluid with diameters $d_1 = 4.96 \times 10^{-4}$ m, $d_2 = 1.25 \times 10^{-4}$ m, $d_3 = 1.0 \times 10^{-4}$ m respectively. The bottom elevation is given by $z_B(x) = 0.2 \exp(-40(x - 0.5)^2)$ m for $x \in [0, L]$, the initial condition for the height is $h(t = 0) = 0.3 - z_B$, and for the concentration of each species

$$\phi_{i,\alpha} = \frac{1}{M} \sum_{\beta=1}^M \phi_{i,\beta}(0, x) \quad \text{for all } i = 1, \dots, 3, u_\alpha(0, x) = 0 \quad \text{for all } \alpha = 1, \dots, M \text{ and all } x \in [0, L],$$

with $\sum_{\beta=1}^M \phi_{1,\beta}(0, x) = 0.05$, $\sum_{\beta=1}^M \phi_{2,\beta}(0, x) = 0.025$, $\sum_{\beta=1}^M \phi_{3,\beta}(0, x) = 0.01$. The sediment concentrations are vertically uniformly distributed at each point x . We use a closed basin as boundary condition.

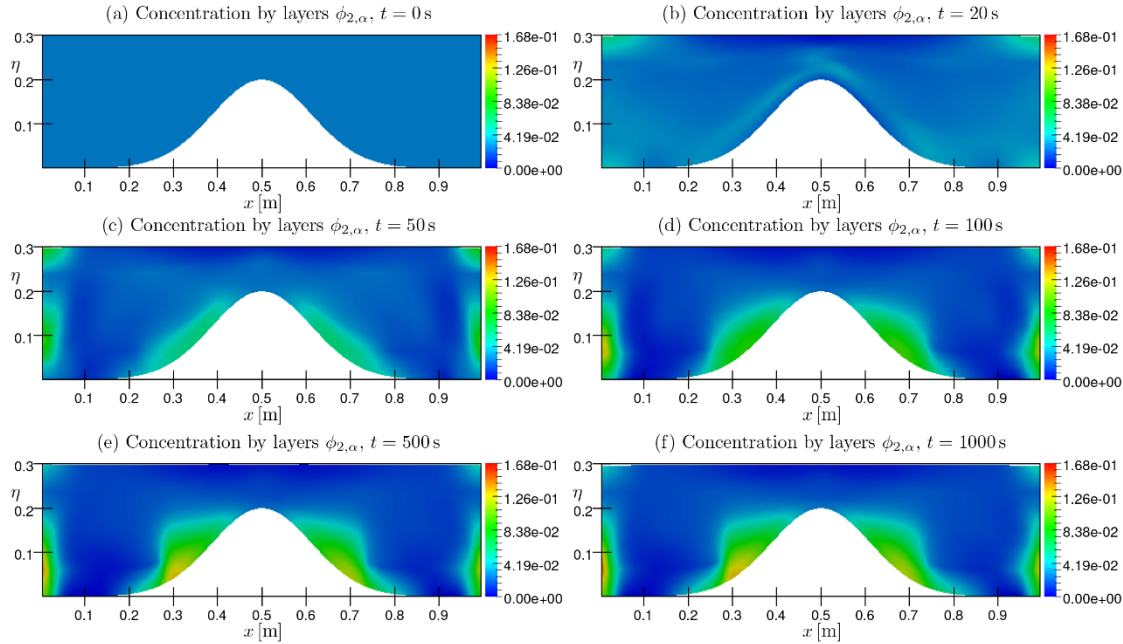


Fig. 11: Example 6: Concentration of ϕ_2 by color in a domain with a bump, $\eta(x) = z_B(x) + h(x)$ m, at simulated times $T = 0$ s, 20 s, 50 s, 100 s, 500 s and $T = 1000$ s.

In Figure 10–12 we can see the concentrations of the each solid species ϕ_1, ϕ_2, ϕ_3 respectively. The behavior of the particles of the different species is what we expected, the bigger particles are deposited faster than other particles over the bottom, in this case to both sides of the bump, where we can find high concentration of species 1 (ϕ_1) in short time, as we can see in Figures 10 (a)–(f). The others smaller particles initially remain in suspension, but at larger simulated times these particles begin to settle and position itself in places where the concentration of species 1 is small (see Figures 11,12). Finally the global behavior of all particles dispersed in the fluid (the sum of the concentrations of the all species) and the velocity field is displayed in Figure 13, in this picture, we can see how these are deposited on the bottom in both side of the bump and also as some particles of species 2 and species 3 are kept in suspension in small concentration yet. In the same figure we show the velocity field of the mixture and its magnitude, which is a consequence of the particles movement. Recirculations appear to both sides of the bump too. In the first times high velocities appear avoiding that some particles settle rapidly. At larger times the velocity decreases and the particles settle.

5 Conclusions

To conclude this contribution, we mention that the issue of hyperbolicity, outlined in Section 2, is still an open problem for some important models of polydisperse sedimentation, including the model by Patwardhan and Tien [42] which is supported by some experimental evidence. On the other hand, the schemes developed for one-dimensional sedimentation can also be applied to other models, for instance to multi-class extensions of the well-known Lighthill-Whitham-Richards kinematic traffic model (see [10,52]). The latter models form a case of the theory of Section 2 for $m = 1$, and admit a separable entropy so that even entropy-stable schemes can be defined [25]. However, no entropy function is known for polydisperse sedimentation models shown here. The mathematical theory is still incomplete.

No well-posedness theory is available for strongly degenerate convection-diffusion systems of the type (DCM). In fact, the IMEX-RK approach is justified by convergence of the scheme to the same solutions

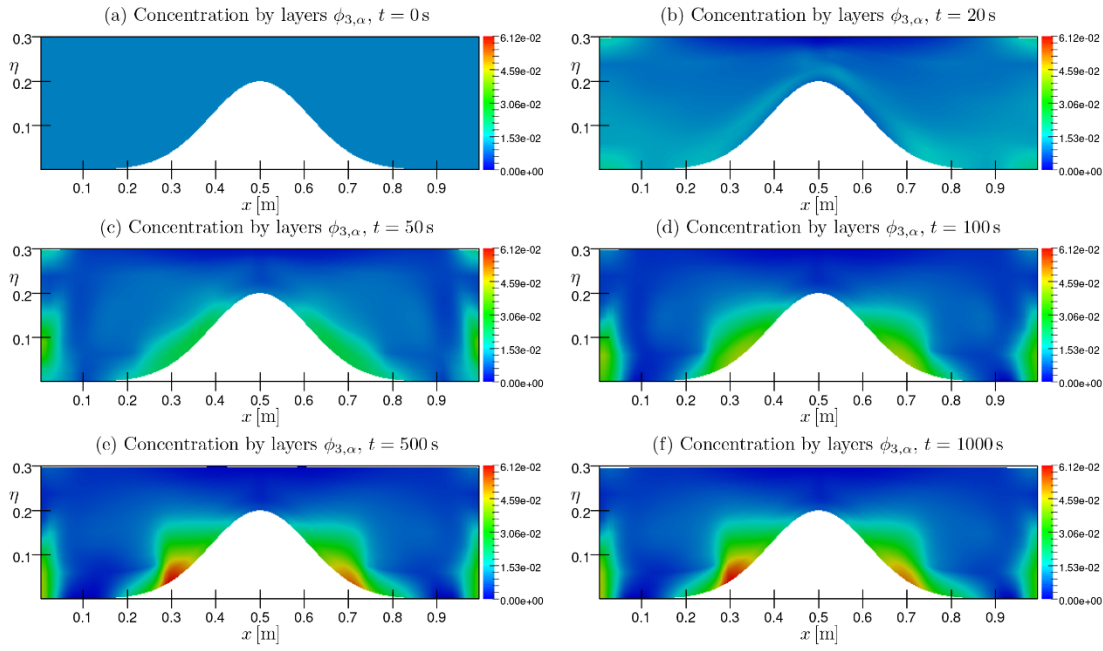


Fig. 12: Example 7: Concentration of ϕ_3 by color in a domain with a bump, $\eta(x) = z_B(x) + h(x)$ m, at simulated times $T = 0$ s, 20 s, 50 s, 100 s, 500 s and $T = 1000$ s.

that are approximate by the KT scheme.

We mention that the multilayer shallow water system for polydisperse sedimentation is currently being extended to two horizontal space dimensions. The current model should be furthermore be refined by mechanisms of sediment erosion and variation of topography due to sediment deposit.

Acknowledgements

RB is partially funded by Fondecyt project 1170473; CRHIAM, project CONICYT/FONDAP/15130015; and CONICYT/PIA/Concurso Apoyo a Centros Científicos y Tecnológicos de Excelencia con Financiamiento Basal AFB170001. VO is supported by Conicyt scholarship.

References

- [1] A. Abeynaike, A.J. Sederman, Y. Khan, M.L. Johns, J.F. Davidson, and M.R. Mackley, The experimental measurement and modelling of sedimentation and creaming for glycerol/biodiesel droplet dispersions, *Chem. Eng. Sci.* **79** (2012), 125–137.
- [2] L.A. Amy, P.J. Talling, V.O. Edmonds, E.J. Sumner, A. and Lesueur, An experimental investigation of sand-mud suspension settling behaviour: implications for bimodal mud contents of submarine flow deposits, *Sedimentology* **53** (2006), 1411–1434.
- [3] J. Anderson, A secular equation for the eigenvalues of a diagonal matrix perturbation, *Linear Algebra Appl.* **246** (1996), 49–70.
- [4] U.M. Ascher, S.J. Ruuth, and R.J. Spiteri, Implicit-explicit Runge-Kutta methods for time-dependent partial differential equations, *Appl. Numer. Math.* **25** (1997), 151–167.

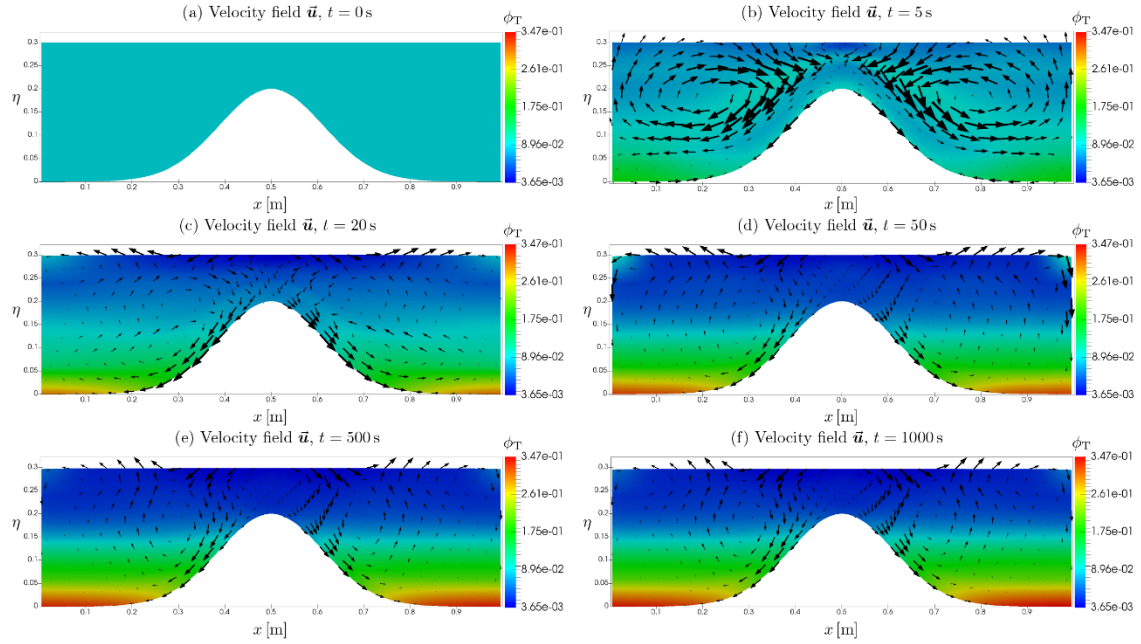


Fig. 13: Example 8: Velocity field \vec{u} over concentration $\phi_T = \phi_1 + \phi_2 + \phi_3$, $\eta(x) = z_B(x) + h(x)m$ in different times.

- [5] E. Audusse, A multilayer Saint-Venant model: derivation and numerical validation, *Discrete Contin. Dyn. Syst. Ser. Bn* **5** (2005), 189–214.
- [6] E. Audusse and M.-O. Bristeau, Finite-volume solvers for a multilayer Saint-Venant system, *Int. J. Appl. Math. Comput. Sci.* **17** (2007), 311–319.
- [7] E. Audusse, M.-O. Bristeau, M. Pelanti, and J. Sainte-Marie, Approximation of the hydrostatic Navier-Stokes system for density stratified flows by a multilayer model: kinetic interpretation and numerical solution, *J. Comput. Phys.* **230** (2011), pp. 3453–3478.
- [8] G.K. Batchelor and R.W. Janse van Rensburg, Structure formation in bidisperse sedimentation, *J. Fluid Mech.* **166** (1986), 379–407.
- [9] G.K. Batchelor and C.S. Wen, Sedimentation in a dilute polydisperse system of interacting spheres. Part 2. Numerical results, *J. Fluid Mech.* **124** (1982), 495–528.
- [10] S. Benzoni-Gavage and R.M. Colombo, An n -populations model for traffic flow, *Eur. J. Appl. Math.* **14** (2003), 587–612.
- [11] S. Berres, R. Bürger, K.H. Karlsen, and E.M. Tory, Strongly degenerate parabolic-hyperbolic systems modeling polydisperse sedimentation with compression, *SIAM J. Appl. Math.* **64** (2003), 41–80.
- [12] S. Berres, R. Bürger, and E.M. Tory, Applications of polydisperse sedimentation models, *Chem. Eng. J.* **111** (2005), 105–117.
- [13] S. Boscarino, R. Bürger, P. Mulet, G. Russo, and L.M. Villada, Linearly implicit IMEX Runge-Kutta methods for a class of degenerate convection-diffusion problems, *SIAM J. Sci. Comput.* **37** (2015), B305–B331.
- [14] ———, On linearly implicit IMEX Runge-Kutta Methods for degenerate convection-diffusion problems modelling polydisperse sedimentation, *Bull. Braz. Math. Soc. (N. S.)* **47** (2016), 171–185.

- [15] S. Boscarino, P.G. Le Floch, and G. Russo, High-order asymptotic-preserving methods for fully nonlinear relaxation problems, *SIAM J. Sci. Comput.* **36** (2014), A377–A395.
- [16] R. Bürger, S. Diehl, M.C. Martí, P. Mulet, I. Nopens, E. Torfs, and P.A. Vanrolleghem, Numerical solution of a multi-class model for batch settling in water resource recovery facilities, *Appl. Math. Modelling* **49** (2017), 415–436.
- [17] R. Bürger, R. Donat, P. Mulet, and C.A. Vega, Hyperbolicity analysis of polydisperse sedimentation models via a secular equation for the flux Jacobian, *SIAM J. Appl. Math.* **70** (2010), 2186–2213.
- [18] ——, On the implementation of WENO schemes for a class of polydisperse sedimentation models, *J. Comput. Phys.* **230** (2011), 2322–2344.
- [19] ——, On the hyperbolicity of certain models of polydisperse sedimentation, *Math. Meth. Appl. Sci.* **35** (2012), 723–744.
- [20] R. Bürger, E.D. Fernández-Nieto, and V. Osores, A dynamic multilayer shallow water model for polydisperse sedimentation. Preprint 2018-13, Centro de Investigación en Ingeniería Matemática, Universidad de Concepción; submitted.
- [21] R. Bürger, K.H. Karlsen, E.M. Tory, and W.L. Wendland, Model equations and instability regions for the sedimentation of polydisperse suspensions of spheres, *ZAMP Z. Angew. Math. Mech.* **82** (2002), 699–722.
- [22] R. Bürger, S. Kumar, and R. Ruiz-Baier, Discontinuous finite volume element discretization for coupled flow-transport problems arising in models of sedimentation, *J. Comput. Phys.* **299** (2015), 446–471.
- [23] R. Bürger, P. Mulet and L.M. Villada, Spectral WENO schemes with Adaptive Mesh Refinement for models of polydisperse sedimentation, *ZAMP Z. Angew. Math. Mech.* **93** (2013), 373–386.
- [24] ——, Regularized nonlinear solvers for IMEX methods applied to diffusively corrected multispecies kinematic flow models, *SIAM J. Sci. Comput.* **35** (2013), B751–B777.
- [25] R. Bürger, H. Torres, and C.A. Vega, An entropy stable scheme for the multiclass Lighthill-Whitham-Richards traffic model, *Adv. Appl. Math. Mech.*, to appear.
- [26] R. Bürger and E.M. Tory, On upper rarefaction waves in batch settling, *Powder Technol.* **108** (2000), 74–87.
- [27] R.H. Davis and H. Gecol, Hindered settling function with no empirical parameters for polydisperse suspensions, *AICHE J.* **40** (1994), 570–575.
- [28] S. Diehl, Shock-wave behaviour of sedimentation in wastewater treatment: a rich problem. In: K. Åström, L.-E. Persson, and S.D. Silvestrov (eds.), *Analysis for Science, Engineering and Beyond*, Springer Proc. in Math. 6, Springer-Verlag, Berlin, Chapter 7, 175–214.
- [29] R. Donat and P. Mulet, A secular equation for the Jacobian matrix of certain multi-species kinematic flow models, *Numer. Methods Partial Differential Equations* **26** (2010), 159–175.
- [30] R.M. Dorrell, A.J. Hogg, and D. Pritchard, Polydisperse suspensions: erosion, deposition, and flow capacity, *J. Geophys. Res.* **118** (2013), 1939–1955.
- [31] R. Dorrell, A.J. Hogg, E.J. Sumner, and P.J. Talling, The structure of the deposit produced by sedimentation of polydisperse suspensions, *J. Geophys. Res.* **116** (2011), paper F01024.
- [32] E.D. Fernández-Nieto, E.H. Koné, T. Morales de Luna, and R. Bürger, A multilayer shallow water system for polydisperse sedimentation, *J. Comput. Phys.* **238** (2013), 281–314.

- [33] M. Gray, Z. Xu, and J. Masliyah, Physics in the oil sands of Alberta, *Physics Today* **62** (2009), No. 3, 31–35.
- [34] L. Pareschi and G. Russo, Implicit-explicit Runge-Kutta schemes and applications to hyperbolic systems with relaxation, *J. Sci. Comput.* **25** (2005), 129–155.
- [35] G.S. Jiang and C.-W. Shu, Efficient implementation of Weighted ENO schemes, *J. Comput. Phys.* **126** (1996), 202–228.
- [36] B.H. Kim and M.S. Klima, Development and application of a dynmaic model for hindered-settling column separations, *Minerals Eng.* **17** (2004), 403–410.
- [37] A. Kurganov and E. Tadmor, New high-resolution central schemes for nonlinear conservation laws and convection-diffusion equations, *J. Comput. Phys.* **160** (2000), 241–282.
- [38] G.J. Kynch, A theory of sedimentation, *Trans. Faraday Soc.* **48** (1952), 166–176.
- [39] X.-D. Liu, S. Osher, and T. Chan, Weighted essentially non-oscillatory schemes, *J. Comput. Phys.* **115** (1994), 200–212.
- [40] M.J. Lockett and K.S. Bassoon, Sedimentation of binary particle mixtures, *Powder Technol.* **24** (1979), 1–7.
- [41] J.H. Masliyah, Hindered settling in a multiple-species particle system, *Chem. Eng. Sci.* **34** (1979), 1166–1168.
- [42] V.S. Patwardhan and C. Tien, Sedimentation and liquid fluidization of solid particles of different sizes and densities, *Chem. Eng. Sci.* **40** (1985), 1051–1060.
- [43] S. Qian, R. Bürger, and H.H. Bau, Analysis of sedimentation biodetectors, *Chem. Eng. Sci.* **60** (2005), 2585–2598.
- [44] J. Sainte-Marie, Vertically averaged models for the free surface non-hydrostatic Euler system: derivation and kinetic interpretation, *Math. Models Methods Appl. Sci.* **21** (2011), pp. 459–490.
- [45] W.K. Sartory, Three-component analysis of blood sedimentation by the method of characteristics, *Math. Biosci.* **33** (1977), 145–165.
- [46] W. Schneider, G. Anestis, and U. Schaflinger, Sediment composition due to settling of particles of different sizes, *Int. J. Multiphase Flow* **11** (1985), 419–423.
- [47] E.B. Shin, H.S. Yoon, Y.D. Lee, Y.S. Pae, S.W. Hong, and B.H. Joo, The effects of particle size distribution on the settleability of CSO pollutants, *Wat. Sci. Tech.* **43** (5) (2001), 103–110.
- [48] C.-W. Shu, High order weighted essentially nonoscillatory schemes for convection dominated problems, *SIAM Rev.* **51** (2009), 82–126.
- [49] C.-W. Shu and S. Osher, Efficient implementation of essentially non-oscillatory shock capturing schemes, *J. Comput. Phys.* **77** (1988), 439–471.
- [50] R. Simura and K. Ozawa, Mechanism of crystal redistribution in a sheet-like magma body: Constraints from the Nosappumisaki and other Shoshonite intrusions in the Nemuro peninsula, Northern Japan, *J. Petrology* **47** (2006), 1809–1851.
- [51] E. Torfs, M.C. Martí, F. Locatelli, S. Balemans, R. Bürger, S. Diehl, J. Laurent, P.A. Vanrolleghem, P. François, and I. Nopens, Concentration-driven models revisited: towards a unified framework to model settling tanks in water resource recovery facilities, *Water Sci. Tech.* **75** (2017), 539–551.
- [52] G.C.K. Wong and S.C.K. Wong, A multi-class traffic flow model?an extension of LWR model with heterogeneous drivers, *Transp. Res. A* **36** (2002), 827–841.
- [53] Y.-T. Zhang and C.-W. Shu, ENO and WENO schemes, Chapter 5 in R. Abgrall and C.-W. Shu (eds.), *Handbook of Numerical Methods for Hyperbolic Problems: Basic and Fundamental Issues*. Handbook of Numerical Analysis vol. 17, North Holland, (2016), 103–122.